Korean J. Chem. Eng., 34(4), 1250-1259 (2017)
DOI: 10.1007/s11814-016-0355-4

pISSN: 0256-1115
eISSN: 1975-7220

Mechanism underlying the effect of conventional drying on the grinding characteristics of Ximeng lignite

Yumeng Yang, Jianzhong Liu†, Xiang He, Zhihua Wang, Junhu Zhou, and Kefa Cen

State Key Lab of Clean Energy Utilization, Zhejiang University, Hangzhou 310027, China
(*Received 14 July 2016 • accepted 20 December 2016*)

Abstract−Same amounts of moisture were removed from Ximeng lignite (XL) with different particle size ranges pretreated at different drying temperatures. The effect of conventional drying on the grindability of the XLs was investigated. Increasing the drying temperature improved the grindability of all the samples. The results of scanning electron microscopy and mercury intrusion porosimetry revealed that the dominant mechanism enhancing the grindability of XL with high moisture was the pore structure destruction induced by the steam jet flow generated with the removal of moisture. Especially, the development of large fractures had a strong connection with the change in the grindability. According to the pore size distribution, the internal structure of the 2.5-4.0 mm coal samples did not develop well under high drying temperature because of the exceedingly short heating time. Therefore, coal particle size, drying temperature, and heating time must be coordinated well to achieve the enhanced drying effect. The grindability of XL had a negative linear correlation with the pore volume fractal dimension, revealing the possibility of fractal dimension for the analysis of lignite grindability.

Keywords: Conventional Drying, Lignite, Grindability, Pore Structure, Fractal Dimension

INTRODUCTION

Low rank coals, occupying nearly half of the reserved coals in the world, have been considered as a potential primary source of energy and chemicals [1]. Lignite is a low-rank coal characterized by high moisture content, low calorific value, and easy spontaneous combustion, which limits its industrial application [2]. Thus, lignite is often used as fuel for pithead power plants or as a chemical raw material. Pulverization is a necessary step in the utilization of raw coal. In fact, the milling system must consume considerable energy, which partly determines the cost of the whole utilization process [3]. The following factors affect coal hardness: coal rank, moisture content, petrography, distribution, and mineral type [4-7]. Among all factors that affect lignite grindability, moisture content is the most easily altered. Dehydration also substantially improves the calorific value of lignite and increases the utilization rate of resources. Thus, dehydrating lignite is a necessary step prior to the substance's intensive processing and further utilization [1].

Many drying methods, including the conventional approach or the use of microwaves or waste-heat gas, are used to dehydrate coal and consequently increase coal grindability [8-11]. The pre-heating treatment of coal samples can induce structural microfractures in coal, which is helpful in improving coal grindability. Marland et al. [12] compared the grindability of microwave-exposed coals to conventionally heated coals. The grindability of coal samples treated at 250 °C for 60 min was increased to about 20%, and similar results were achieved when the coal sample was treated for only 3 min under microwave irradiation. Zhu et al. [13] compared the different effects of conventional heating and microwave irradiation on lignite grindability. After 0.5 min of microwave irradiation, the grindability of the coal sample was increased by 44.03%, and the moisture content became 29.66%. By contrast, the coal sample treated at 150 °C for 20 min attained an increment in grindability by 39.91% and a moisture content of 24.63%. Given these findings, researchers pointed out that the speed of moisture removal is the more important factor in the dehydration process for improving the grindability of high-moisture-content coal. Lester et al. [14] investigated the grindability changes of coal samples exposed under 8 kW microwave irradiation for 0.1 s. Results showed that although residence times were short, the grindability of each coal sample was increased substantially. Furthermore, the exceedingly short residence times rendered the effects on the petrographic and chemical characteristics negligible. When the coal samples are heated by microwave, the moisture within the coal particle is transferred from the internal structure to the external environment by steam-pressure-driven jet flow [15]. The jet flow destroys the pore structure of the coal particles, thereby improving coal grindability. Therefore, given its internal heating characteristic, microwave irradiation achieves a higher dehydration rate and affects the coal sample to a significantly greater extent than those in conventional drying.

The behavior of porous materials in comminution processes is strongly affected by porosity type, which may be characterized by different void shapes and interconnection degrees [16]. As a typical porous material, lignite exhibits a breakage behavior closely connected to its inherent internal pore structure. Fractal geometry provides a new perspective for studying the irregular microscopic

†To whom correspondence should be addressed.
E-mail: jzliu@zju.edu.cn, loveowen@zju.edu.cn
‡This paper is reported in the 11th China-Korea Clean Energy Workshop.

pore structure of coal samples. Moreover, considerable work has been achieved in applying fractal geometry to the study of coal micropore structures. For instance, Mahamud and Novo [17] investigated the fractal characterization of four bituminous coals and the corresponding coal sample oxidized in air at 543 K for different time periods. Fractal dimensions calculated with different methods similarly changed and were sensitive to oxidation treatment. The evolution of the fractal dimension of coals with oxidation was controlled by two dominant mechanisms: the oxidation of the pore surface and the access of mercury to previously non-accessible regions. Cheng et al. [18] studied the pore fractal structures and combustion dynamics of cokes derived from the pyrolysis of 18 typical Chinese power coals using low-temperature nitrogen absorption. They found that the cokes derived from lignite pyrolysis possessed larger pore fractal dimensions, and therefore achieved lower ignition temperatures and higher burnout efficiencies than those from lean coal and anthracite pyrolysis. Hu et al. [19] analyzed the surface structures of parent coal and char with different burn-off ratios. They introduced fractal theory to scanning electron microscopy (SEM) image analysis and utilized the particle surface fractal dimension to quantitatively describe the surface character of the coal/char particles. The particle surface fractal dimension (D_{ps}) was determined by SEM image analysis, whereas the internal surface fractal dimension (D_s) was determined by N_2 isotherm adsorption/desorption. With increasing carbon burn-off ratios, the D_{ps} initially increased and then decreased. The changes in D_s of the three Chinese coals were similar to their S_{BET} development. As discussed above, fractal theory has a strong ability to describe irregular coal structure.

Although various drying methods have been used to improve coal grindability, few have paid attention to the relationship between the specific development status of fractures in the coal body and grindability changes. Given its high dehydration rate, microwave irradiation offers a more significant influence on coal grindability than other methods. Hence, we adopted the conventional heating method to allow Ximeng lignites (XLs) lose the same quantity of moisture at different temperatures. Different dehydration rates were achieved for each sample, and the effects of different dehydration rates on the grindability of the XLs were investigated. Based on the experiment of SEM, mercury intrusion porosimetry, and fractal theory, the controlled mechanisms of the increment in the grindability of XLs treated by different temperatures were discussed. This study aimed to provide references for processing and utilizing XLs.

EXPERIMENTAL

1. Materials

The lignite used in this study was derived from the Ximeng region of Inner Mongolia, which is the largest producer of lignite in China. Naturally dried XLs were crushed using a jaw crusher and then screened into three mono size ranges (1.0-1.6, 1.6-2.5, and 2.5-4.0 mm) by a standard sieve. The proximate analysis for the coal is given in Table 1. Details of the proximate changes were not included in this paper because such changes, except in moisture content, were found negligible. Moreover, moisture content is a controlled variable in this experiment, that is, all the samples lost the same quantity of moisture.

Table 1. Proximate analysis of the sample

Coal sample	M_{ad} (%)	A_{ad} (%)	V_{daf} (%)	FC_{daf} (%)	$Q_{b,ad}$ (J/g)
XL	25.82	11.67	47.65	52.35	18122

2. Methods

2-1. Conventional Drying Experiments

Conventional drying experiments were carried out on an electronic moisture analyzer (MA35, Sartorius group, German). Samples were heated by two powerful metal, tubular-shaped heating elements (also called dark radiators). Uniform distribution of the heat rays was achieved by using an integrated reflector. Sample quality was monitored momentarily with the thermogravimetric method, allowing us to quantitatively remove moisture by controlling the heating time. During the conventional drying experiments, 20 g of XL was uniformly spread in a disposable sample pan and then dehydrated under different temperatures (50 °C, 80 °C, 110 °C, and 140 °C) until 20% of their total quantity was lost and changed to 16 g. Three mono size ranges (1.0-1.6, 1.6-2.5, and 2.5-4.0 mm) were adopted, and each size was treated under four temperature conditions. Thus, 12 groups of experiments were carried out.

2-2. Grindability Tests

A frequency conversion planetary ball mill (XQM-2L, Nanjing Kexi Instruments Research Institute, China) was used to grind both the treated and untreated XLs. During the grindability tests, the mill consisted of two 500 mL steel cylinders with six steel balls of 2 cm diameter inside each cylinder. These balls freely move up and down at the designed operating speed. Approximately 16 g of XL was uniformly spread in each steel cylinder. The revolution velocity of the grail was 100 rpm, and the rotation velocity of the steel cylinder was 200 rpm. The operating condition was determined after numerous pre-experiments. The grinding times of the XLs were set to 20, 40, 60, 80, and 100 s. The ground product was sieved to obtain the top size fraction of each mono size range sample (i.e., after milling the particles whose size is still in 2.5 to 4.0 mm range are the top size fraction of the 2.5-4.0 mm samples). Each particle size fraction was weighed, and the corresponding mass fraction was calculated.

Grindability is the level of difficulty for particles to be pulverized in milling process. After grinding different materials under the same conditions, the particle size distribution of the milled materials would represent the 'grindability'. The better grindability the material has, the more fine particles there will be. The grindability can be expressed as a numeric value by weighing the mass of different particle size. For example, in the Hardgrove Grindability Index (HGI) test, the sample is sieved and weighed to determine the mass of −75 μm fraction after milling. By comparing the mass of −75 μm fraction with the calibration chart, the HGI of coal is determined [20]. The breakage rates of the coal samples (S_i) of certain particle size fractions are different at each particle size and can be acquired through grinding tests. Previous studies [21,22] showed that S_i corresponds to a certain particle size fraction that can be used to evaluate coal sample grindability and connects with

the HGI. Higher breakage rates result in better grindability. Once effective breakage occurs in the mill, the breakage rate can be modeled on the basis of first-order grinding kinetics. When considering only the top size fraction, the simplest expression that can be used to calculate the breakage rate S_1 is shown in the following equation [21]:

$$\ln\left(\frac{w_1(t)}{w_1(0)}\right) = S_1 \times t, \quad (1)$$

where t is the grinding time (min); $w_1(0)$ is the relative amount of the top size particles in the mill at time 0, which is 100%; $w_1(t)$ is the mass fraction of the top size particles in the mill at time t (%); and S_1 is the breakage rate of the top size particles (min^{-1}). Therefore, the breakage rate S_1 can be calculated by plotting the natural logarithm of the relative amount of top size particles against the grinding time. The slope of the straight line should be equal to S_1.

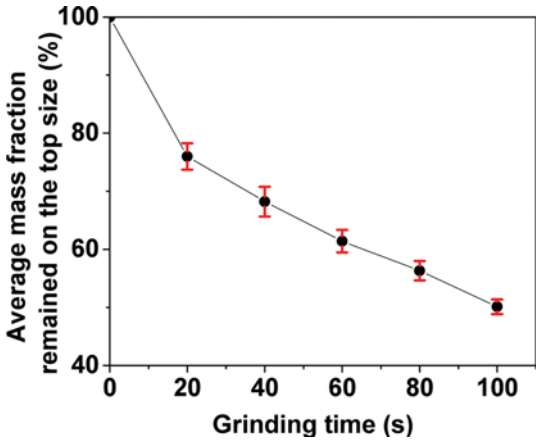

Fig. 1. Variation in breakage behavior of raw coal with size fraction 2.5-4.0 mm.

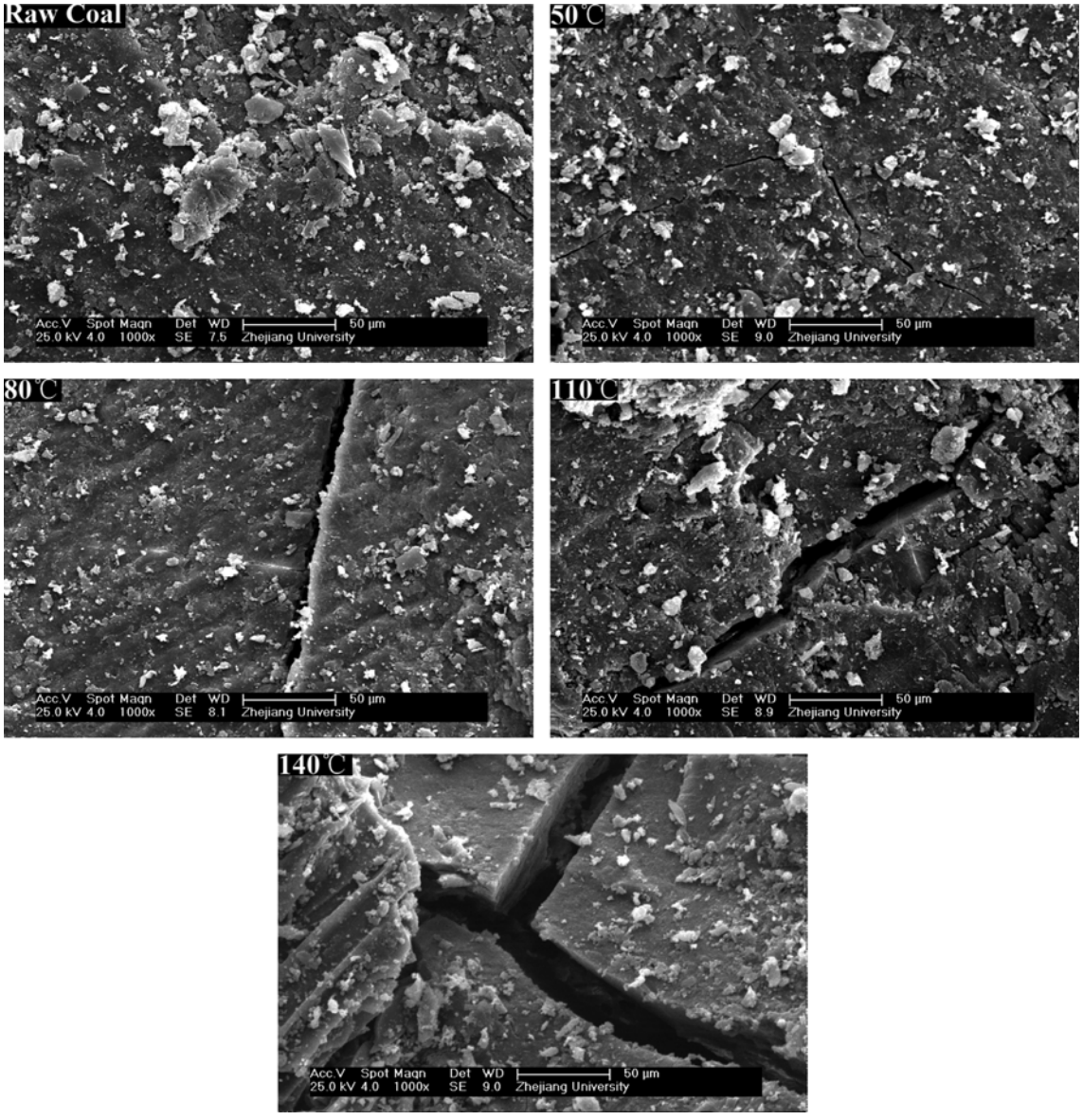

Fig. 2. SEM images of untreated and heated coal samples at 2.5-4.0 mm.

2-3. SEM and Mercury Injection Experiments

The surface micro-topography of the XLs was measured by SEM (SIRION-100, FEI, Netherlands).

Mercury intrusion porosimetry (MIP) data were obtained on an automatic mercury porosimeter (AutoPore IV 9510, Micromeritics, USA). All samples were dried at 50 °C in a vacuum drying oven before determination to ensure the absence of moisture in the samples during the mercury injection experiments.

2-4. Calculation of Fractal Dimension

To overcome the interfacial tension between the mercury and the solid, a pressure P(r) must be exerted on the mercury before the mercury fills a pore of size r. For a cylindrical pore, P and r are related by the well-known Washburn equation [23]. According to this equation and the Menger Sponge fractal model, the fractal dimension can be calculated with the following equation [17,24]:

$$\ln\left(\frac{dV}{dP}\right) \propto (D-4)\ln P, \quad (2)$$

where P is the pressure, V is the cumulative intrusion volume that corresponds to P, and D is the fractal dimension. The fractal dimension of the surface of the porous medium can then be obtained simply from the slope of the ln-ln plot of dV/dP versus P.

RESULTS AND DISCUSSION

1. Repetitive Experiments

The data accuracy of the grindability tests directly affects the S_1 calculation. Therefore, the reproducibility of the sample grindability should be considered. In this study, the particle size range of XL with size fraction 2.5-4.0 mm was the widest and likely increased sampling error. Consequently, four 16 g XLs of size fraction 2.5-4.0 mm were ground for 20, 40, 60, 80, and 100 s, respectively. As shown in Fig. 1, the reproducibility of the sample grindability lay within the range ±2.57%, indicating that the grindability test data were highly reliable.

2. SEM Characterization

SEM analyses of the treated and untreated XLs were helpful in understanding the effects of different drying methods on the physical structure of XLs. The surface of the raw coal was smoother and had fewer cracks than the treated samples (Fig. 2). After processing in different drying temperatures, fractures and cracks were induced in the treated XLs because of thermal stress or steam jet flow. The different drying temperatures or different dehydration rates exerted varying effects on the physical structural damage in the XLs. Higher drying temperatures resulted in more microfractures and cracks, as shown in the image. The cracks in the treated XLs enhanced the samples' grindability [14,22].

3. Grindability Tests

With increasing grinding time, the mass fraction on the top size of the XLs decreased sharply at the beginning (Fig. 3). Meanwhile, Fig. 4 shows the relationships between the natural logarithm of the oversized mass fraction and grinding time for all samples. The slopes obtained by linear fit corresponded to the breakage rates of the top size particles for the XLs (Table 2). The corresponding R^2

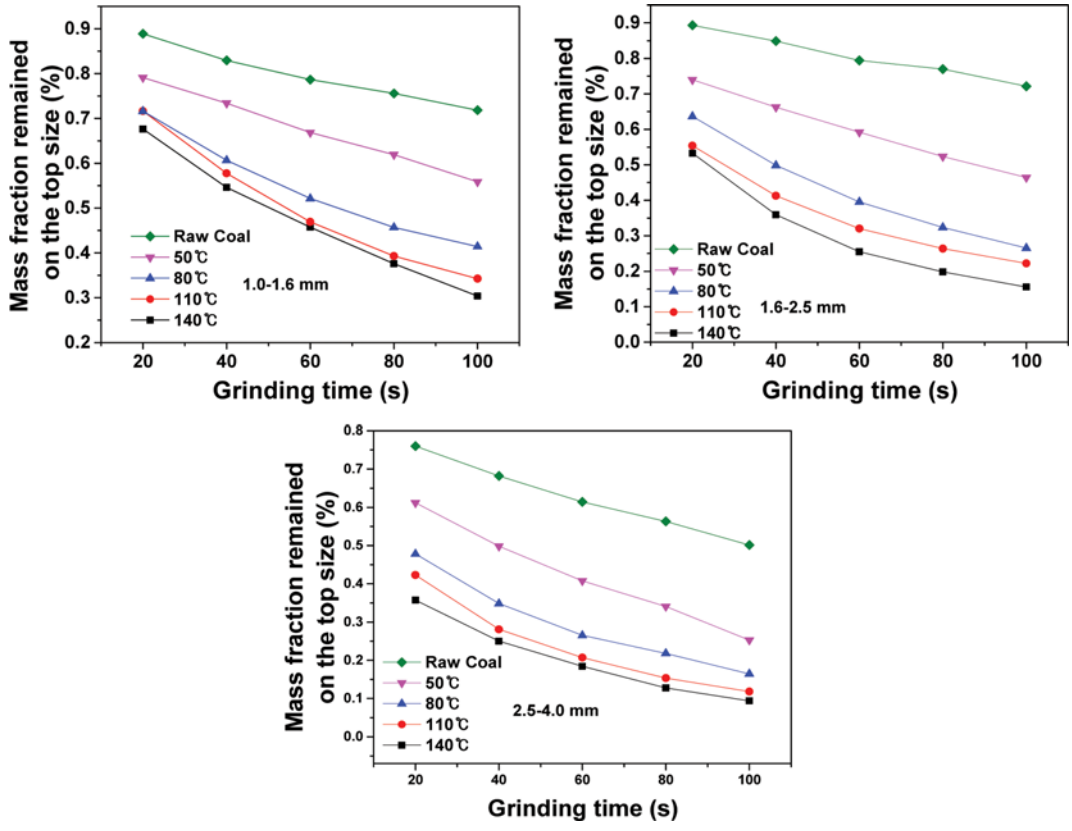

Fig. 3. Relationship between remaining mass fraction and grinding time for all samples.

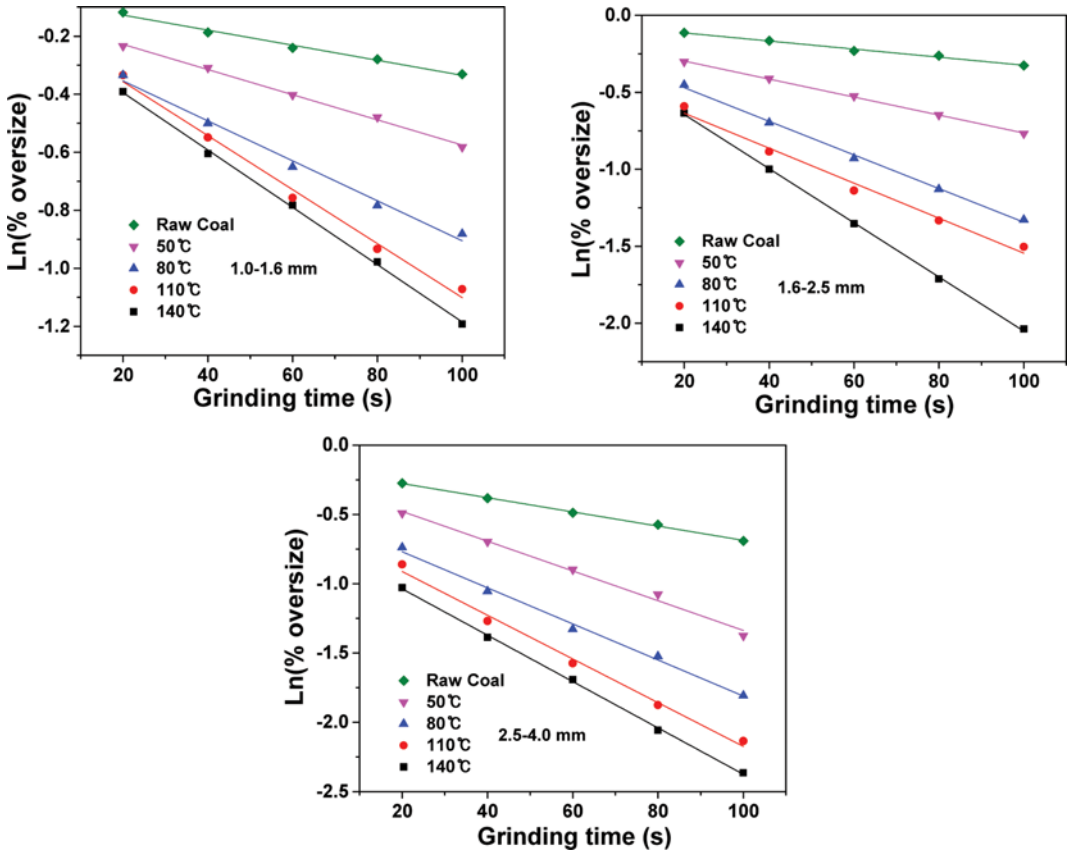

Fig. 4. Natural logarithm of the oversized percentage against grinding time for all samples.

Table 2. Specific rate of breakage data (S_1) for all samples

Coal sample	Drying condition (°C)	S_1 (s^{-1})	Increment in grindability (%)	R^2
1.0-1.6 mm	Raw coal	0.00259	0	0.9870
	50	0.00433	67.18	0.9963
	80	0.00689	166.02	0.9877
	110	0.00930	259.07	0.9903
	140	0.00988	281.47	0.9988
1.6-2.5 mm	Raw coal	0.00263	0	0.9886
	50	0.00584	122.05	0.9993
	80	0.01092	315.21	0.9969
	110	0.01136	331.94	0.9823
	140	0.01759	568.82	0.9995
2.5-4.0 mm	Raw coal	0.00512	0	0.9979
	50	0.01073	109.57	0.9891
	80	0.01302	154.30	0.9924
	110	0.01577	208.01	0.9904
	140	0.01672	226.56	0.9989

values were higher than 0.98, which indicated good fit (Table 2, Fig. 4). The breakage rates of the heat-treated XLs of different particle size ranges increased with rising heating temperature. The increment in grindability of each treated sample is calculated by the following method: using its breakage rate to be divided by the raw coal's breakage rate, after that using the quotient subtract 100% and the result is the increment in grindability.

When the heating temperature was 140 °C, the increment in grindability of the heat-treated XL increased from 226.56% in the 2.5-4.0 mm particle size range to 568.82% in the 1.6-2.5 mm particle size range. In contrast, the increment in grindability of all the samples treated under 50 °C was much less than those of the oth-

Table 3. Dehydration time for all samples

Coal sample	1.0-1.6 mm				1.6-2.5 mm				2.5-4.0 mm			
Drying condition (°C)	50	80	110	140	50	80	110	140	50	80	110	140
Dehydration time (min)	57	21	12	8.9	63	22	11	9.4	97	26	12	10

ers. The dehydration time of 50 °C was at least twice longer than under 80 °C (Table 3). When the heating temperature was 50 °C, the dehydration time of the coal sample was much slower than that in other conditions. Hence, dehydration rate is an important condition that affects the increment in coal grindability. At constant temperature, smaller particle sizes had higher dehydration rates (Table 3). This result can be explained by the notion that smaller coal particle sizes provide larger specific surface areas and hence, higher efficiency in thermal conductivity.

Coal samples of different particle sizes treated under different temperatures showed different grinding behaviors and comminuting characters. This result was attained because of the variation in the development of internal fractures (pore structure) among the coal samples. A quantitative analysis of coal sample internal fractures was performed through the mercury injection experiment, and the relationship between fracture development and grindability would be explained in the following section.

4. Relationship between Pore Characteristics and Grindability

4-1. Pore Distribution Characteristics

Given the MIP experiments, if the pressure was less than 0.5 MPa (corresponding to a pore diameter larger than 24,000 nm), the increase in pore volume was primarily due to mercury intrusion into the inter-particle voids, and the surface or internal pores could not be observed at these pressures. Thus, 24,000 nm (0.5 MPa) was regarded as the upper limit. When the pressure exceeded 100 MPa, the corresponding pore diameter was smaller than 13 nm. But because the non-continuous measurement of the mercury intrusion porosimeter used in the experiment, its measuring points were concentrated in 3-6 nm at this time. In this diameter, the mercury was immersed in the gap between molecules; hence, pores of this size could not stand the fracture development caused by dehydration. Thus, 13 nm (100 Mpa) was considered as the lower limit. The porosity of this range (13-24,000 nm) was basically around 10% (Table 5). This result indicates that the pores in this range, as the internal structure of coal, were stable.

The operation of the mercury intrusion porosimeter was divided into two steps of high and low pressures, generating an obvious discontinuity in data point between the two steps for each sample. The parting point (3,850 nm) of the high and low pressures was denoted as the first segmentation point of the research range (13-24,000 nm). The term "micropore" is now reserved for pores not wider than ~2 nm. The wider pore range of 2-50 nm, which were particularly significant in the context of capillary condensation, were designated as mesopores, and those wider than 50 nm were called macropores [25]. Results of mercury injection experiments show that the pore distribution of all coal samples in the 50 nm place was not continuous as usual. The 50 nm value corresponded to another discontinuity point in the pore distribution in coal. Thus, the 50 nm point was regarded as the second segmentation point of the research range. Finally, the research range (13-24,000 nm) was

Table 4. Proportion of the three types of fracture for all samples

Coal sample	Drying condition (°C)	Large fracture (%)	Medium fracture (%)	Small fracture (%)
		3,850 nm<d<24,000 nm	50 nm<d<24,000 nm	13 nm<d<24,000 nm
1.0-1.6 mm	50	16.0314	57.8630	26.1056
	80	18.2006	59.8075	21.9919
	110	18.7464	61.7124	19.5413
	140	20.3553	62.2858	17.3588
1.6-2.5 mm	50	16.0891	62.9570	20.9539
	80	18.5033	61.7726	19.7241
	110	19.7124	61.9299	18.3577
	140	22.1042	61.5957	16.3001
2.5-4.0 mm	50	16.7263	55.8925	27.3812
	80	20.1601	57.8378	22.0021
	110	23.0069	50.1948	26.7983
	140	26.3324	52.1181	21.5494

Table 5. Porosity for all samples (13 nm<d<24,000 nm)

Coal sample	1.0-1.6 mm				1.6-2.5 mm				2.5-4.0 mm			
Drying condition (°C)	50	80	110	140	50	80	110	140	50	80	110	140
Porosity (%)	10.14	10.69	11.76	11.63	11.22	11.01	12.30	11.75	9.69	10.57	10.18	10.00

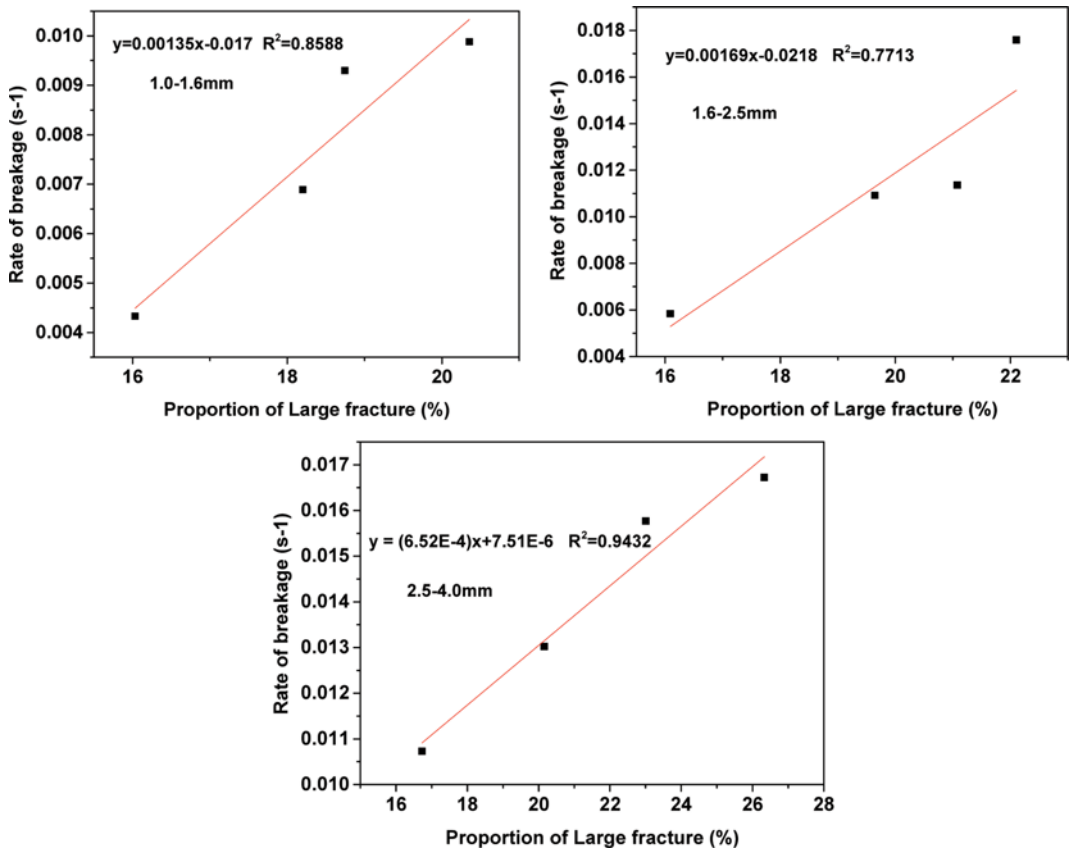

Fig. 5. Linear fitting of the proportion of large fractures and breakage rates.

divided into three parts: 13-50 nm (called small fracture in this paper), 50-3,850 nm (medium fracture), and 3,850-24,000 nm (large fracture). Table 4 lists the proportion of the three fracture types in the range of 13<d<24,000 nm.

The large fracture proportion in all the coal samples increased with increasing heating temperature. The linear fitted curves of the large fracture's proportion and the breakage rates of samples of all particle sizes are shown in Fig. 5. The corresponding R^2 values were at least higher than 0.77, which indicated good fit. This result means that the grindability of the XLs was strongly influenced by the proportion of large fractures. For a certain size of XL, higher heating temperature and dehydration result in larger proportions of large fractures, consequently enhancing grindability.

The proportion of medium fractures was related to both heating temperature and the particle size of the coal sample. For the XLs of 1.0-1.6 mm particle size, the proportion of medium fractures increased with augmenting heating temperature. This result indicates that when the particle size was small, the sample remained heated thoroughly despite the progressive shortening of the heating time. The medium fracture in the internal portion of coal may develop well. For the 1.6-2.5 mm XLs, the proportion of medium fractures was substantially unchanged with increasing heating temperature. The fractal feature of XL, or self-similarity, is discussed in the next section of this paper. Larger fractures were mainly developed from the smaller fractures. Therefore, although such proportion was not considerably altered, the proportion of large fractures increased and hence enabled the medium fractures to develop and compensate for large fractures. This result suggests that with the rise in heating temperature, the heating time was shortened, but the 1.6-2.5 mm XLs may still have been heated thoroughly. For the 2.5-4.0 mm XLs, the proportion of medium fractures slightly increased when the heating temperature changed from 50 °C to 80 °C. However, the continued increment in heating temperature beyond such point decreased the proportion of medium fractures. This observation was achieved because during conventional drying, heat transfers from the surface of the sample to the internal part through conduction, which gradually increases the sample temperature. Short heating times and large particle sizes may lead to insufficient and uneven heating of the whole coal particle. This occurrence may cause the coal particle to dry only on its surface, leaving the core with considerable moisture. When breaking this kind of partly dried coal, the break will probably occur only on the surface. Only surface comminution will probably occur but not the volume comminution, which is unfavorable for further pulverization. Therefore, in actual production, coal particle size, heating temperature, and heating time must be coordinated well to achieve improved drying effects and successful and easy coal particle pulverization.

With rising heating temperature, the proportion of small fractures shrank, except for the 2.5-4.0 mm XLs treated under 80 °C and 110 °C. The porosity did not substantially vary; hence, the decreased proportion of the smallest structure in the research range

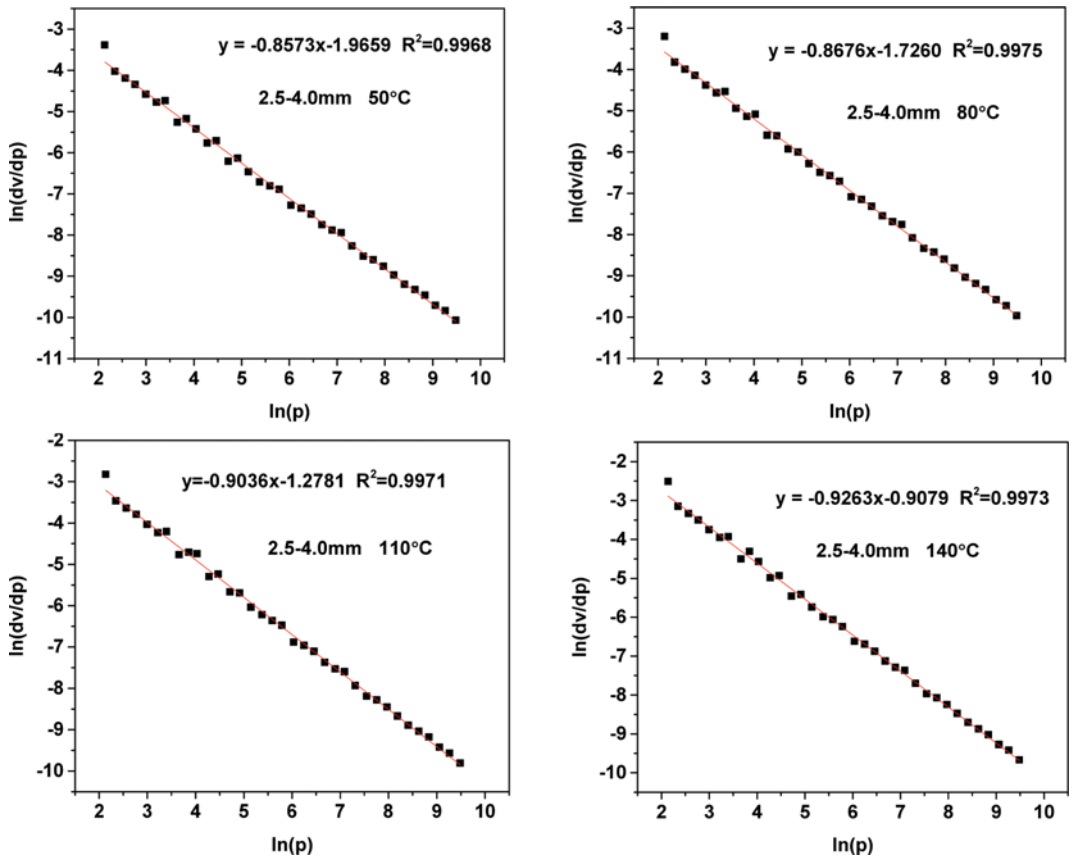

Fig. 6. Fractal fitting curves of mercury porosimetry data in the pressure range 0.5-100 MPa.

implies that the whole pore structure has developed. In particular, the small fractures developed into larger fractures. With the increase in heating temperature, large fractures developed, thereby destroying the structural strength of the coal sample, which importantly determines the enhanced grindability of XLs.

4-2. Pore Fractal Characteristics

In the range of 13-24,000 nm, all the samples showed fractal behavior, as described by the model in Eq. (2). The corresponding R^2 values were all higher than 0.99, which indicated good fit. Given the space limitation, not all the fitting images are shown in this paper. Fig. 6 shows the data plotted in the form ln(dV/dP) versus ln(P) for the 2.5-4.0 mm particle size samples. The detailed data for all the samples are listed in Table 6. The fractal dimension of all the samples was higher than 3. These values are non-physical from a geometric perspective, but merely describe the heterogeneity of the pore structure from the mathematical viewpoint. Friesen et al. [24] studied the fractal dimension of low-ranked coal and found that at pressures higher than about 12 MPa, the fractal dimensions for both samples undergo drastic changes to values D>3. The group believed that this finding was achieved because the increase in the volume of intruding mercury, as measured by MIP at high pressures, was due to a decrease in bulk volume during sample compression rather than to any sampling of the surface pores. Lai and Wang [26] investigated the fractal characteristics of tight gas sandstones using high-pressure mercury intrusion techniques. In their experiment, the calculated fractal dimension was larger than 3.0 in the large-scale range (4.2 to 9.5; average, 6.4); the pore structure referring to large pores became more complex. They speculated that the longer microfractures and larger macropores connected by microfractures cannot be simply assumed to comprise a cylindrical shape. Hence, the pressure remained low, but the fractal dimension was much larger than 3. Li et al. [27] found that the fractal dimensions of geysers rocks are mostly larger than 3. They emphasized that the fractal dimension

Table 6. Fractal dimension and fitting precision data for all samples

Coal sample	Drying condition (°C)	Fractal dimension (D)	R^2
1.0-1.6 mm	50	3.1125	0.9974
	80	3.0941	0.9968
	110	3.0807	0.9975
	140	3.0784	0.9974
1.6-2.5 mm	50	3.1305	0.9971
	80	3.1111	0.9969
	110	3.1292	0.9971
	140	3.0897	0.9971
2.5-4.0 mm	50	3.1427	0.9968
	80	3.1324	0.9968
	110	3.0964	0.9966
	140	3.0747	0.9954

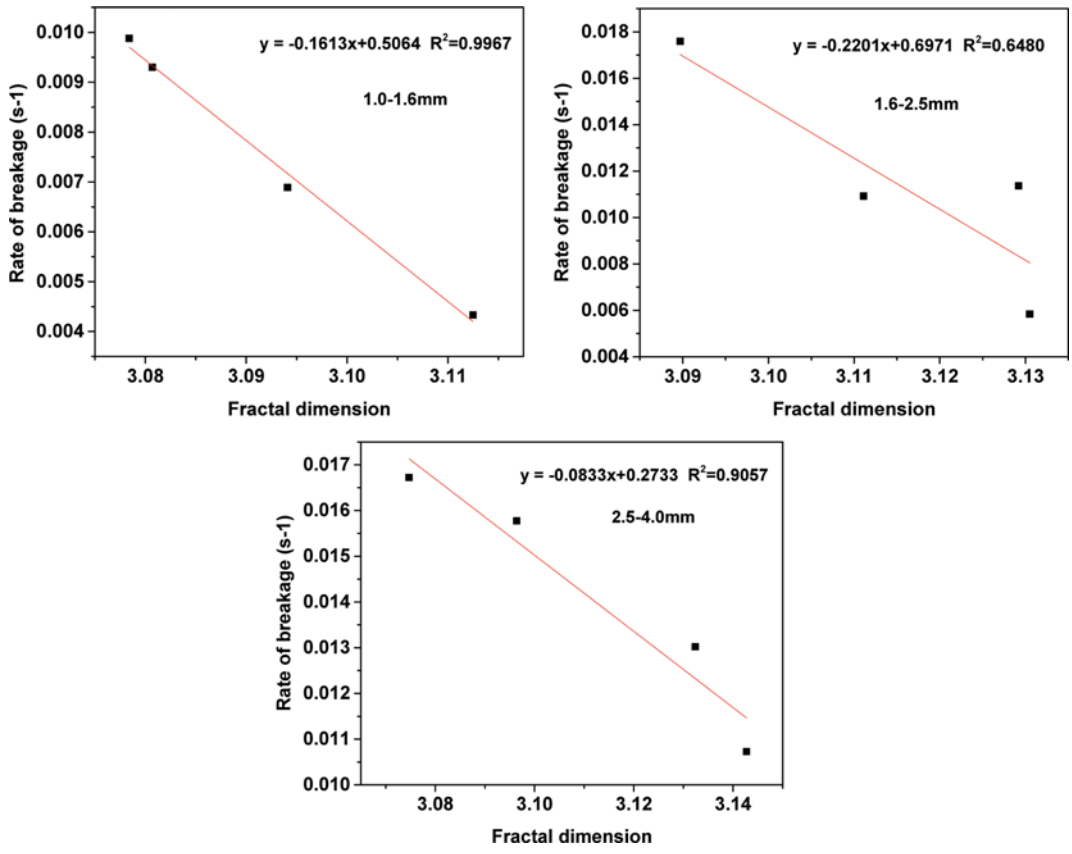

Fig. 7. Linear fitting of the fractal dimension and the breakage rate.

values may differ if various fractal models or approaches are used to match capillary pressure data. However, this notion would not change the relationship between fractal dimension and heterogeneity. In other words, larger fractal dimensions result in greater heterogeneity.

For each particle size of the XLs, the fractal dimensions decreased with rising heating temperature (Fig. 6). Related to the relationship between heating temperature and grindability, we conclude that smaller fractal dimensions generate better XL grindability (Fig. 7). In essence, limited space (the porosity of all samples did not substantially vary) was filled with large fractures when the heating temperature was high, such that the heterogeneity was lower than the space filled with small fractures. This phenomenon indicates that when heating temperature is increased, the fractal dimension of XLs is lowered, a finding consistent with the above-mentioned notions.

The grindability of the XLs was closely connected to pore structure, and the experiments proved that the fractal dimension of XLs could well reflect its pore structure. Hence, a method that uses fractal dimension to express XL grindability should be developed. Furthermore, this method is related to the mechanism underlying grindability changes and could therefore better indicate lignite grindability than other methods.

CONCLUSIONS

The grindability of XL can be dramatically improved by conventional drying at different drying temperatures. The physicochemical analysis results showed that the dominant mechanism enhancing the grindability of XL with high moisture under conventional drying was the pore structure destruction induced by the steam jet flow generated with the removal of moisture. With the increase in the drying temperature, the increment in the grindability of the 1.6-2.5 mm coal sample was the highest, whereas that of the 2.5-4.0 mm coal sample was the lowest. According to the pore structure analysis, the presence of the large fractures within XL resulted in the better grindability. The internal structure of XL was not fully developed because the heating time was exceedingly short for the 2.5-4.0 mm coal sample pretreated at 140 °C, affecting its further pulverization. Therefore, coal particle size, heating temperature, and heating time should be coordinated well to achieve an economical and efficient drying process. The fractal analysis of the internal pore structure revealed that there was a negative linear correlation between the fractal dimension and the grindability of XL.

ACKNOWLEDGEMENT

The authors wish to acknowledge the financial support provided by the National Key Research and Development Plan (Grant No. 2016YFB0600505).

REFERENCES

1. M. Yi and J. W. Lee, *Korean J. Chem. Eng.*, **33**, 3401 (2016).

2. H. Choi, W. Jo, S. Kim, J. Yoo, D. Chun, Y. Phim, J. Lim and S. Lee, *Korean J. Chem. Eng.*, **31**, 2151 (2014).
3. S. W. Kingman and N. A. Rowson, *Miner Eng.*, **11**, 1081 (1998).
4. B. Csöke, L. Bokányi, J. Bõhm and S. Pethö, *Appl. Energy*, **74**, 359 (2003).
5. D. Životić, A. Bechtel, R. Sachsenhofer, R. Gratzer, D. Radić, M. Obradović and K. Tojanović, *Int. J. Coal. Geol.*, **131**, 344 (2014).
6. H. B. Vuthaluru, R. J. Brooke, D. K. Zhang and H. M. Yan, *Fuel Process Technol.*, **81**, 67 (2003).
7. S. C. Chelgani, J. C. Hower, E. Jorjani, S. Mesroghli and A. h. Bagherieh, *Fuel Process Technol.*, **89**, 13 (2008).
8. E. Lester, S. Kingman and C. Dodds, *Fuel*, **84**, 423 (2005).
9. P. C. Harrison and N. A. Rowson, *I Chem. E Res. Event*, **38**, 292 (1997).
10. S. Marland, B. Han, A. Merchant and N. Rowson, *Fuel*, **80**, 1839 (2001).
11. J. Lytle, N. Choi and K. Prisbrey, *Int. J. Miner Process.*, **36**, 107 (1992).
12. S. Marland, B. Han, A. Merchant and N. Ravson, *Fuel*, **79**, 1283 (2000).
13. J. F. Zhu, J. Z. Liu, J. H. Wu, J. Cheng, J. H. Zhou and K. F. Cen, *Fuel*, **162**, 305 (2015).
14. E. Lester, S. Kingman and C. Dodds, *Fuel*, **84**, 423 (2005).
15. J. F. Zhu, J. Z. Liu, J. H. Wu, J. Cheng, J. H. Zhou and K. F. Cen, *Fuel Process Technol.*, **130**, 62 (2015).
16. P. Bevilacqua and G. Ferrara, *Int. J. Miner Process.*, **95**, 117 (1996).
17. M. M. Mahamud and M. F. Novo, *Fuel*, **87**, 222 (2008).
18. J. Cheng, X. Wang, T. Si, F. Zhou, J. H. Zhou and K. F. Cen, *Fuel Process Technol.*, **149**, 49 (2016).
19. S. Hu, M. Li, J. Xiang, L. Sun, P. Li, S. Su and X. Sun, *Fuel*, **83**, 1307 (2004).
20. W. Zuo, Y. Zhao, Y. He, F. Shi and C. Duan, *Int. J. Mining Sci. Technol.*, **22**, 121 (2012).
21. E. L. And and S. Kingman, *Energy Fuel*, **18**, 140 (2004).
22. S. Samanli, *Fuel*, **90**, 659 (2011).
23. X. Wang and R. He, *Korean J. Chem. Eng.*, **24**, 466 (2007).
24. W. I. Friesen and R. J. Mikula, *J. Colloid Interface Sci.*, **120**, 263 (1987).
25. K. S. W. Sing and R. T. Williams, *Adsorpt. Sci. Technol.*, **22**, 773 (2004).
26. J. Lai and G. Wang, *J. Nat. Gas Sci. Eng.*, **24**, 185 (2015).
27. K. Li and R. N. Horne, *Geothermics*, **35**, 198 (2006).